J Biomol NMR (2010) 47:271–282
DOI 10.1007/s10858-010-9430-z

ARTICLE

Nitrogen-detected CAN and CON experiments as alternative experiments for main chain NMR resonance assignments

Koh Takeuchi · Gregory Heffron · Zhen-Yu J. Sun · Dominique P. Frueh · Gerhard Wagner

Received: 26 April 2010 / Accepted: 1 June 2010 / Published online: 17 June 2010

Abstract Heteronuclear direct-detection experiments, which utilize the slower relaxation properties of low γ nuclei, such as ^{13}C have recently been proposed for sequence-specific assignment and structural analyses of large, unstructured, and/or paramagnetic proteins. Here we present two novel ^{15}N direct-detection experiments. The CAN experiment sequentially connects amide ^{15}N resonances using $^{13}C^{\alpha}$ chemical shift matching, and the CON experiment connects the preceding $^{13}C'$ nuclei. When starting from the same carbon polarization, the intensities of nitrogen signals detected in the CAN or CON experiments would be expected four times lower than those of carbon resonances observed in the corresponding ^{13}C-detecting experiment, NCA-DIPAP or NCO-IPAP (Bermel et al. 2006b; Takeuchi et al. 2008). However, the disadvantage due to the lower γ is counteracted by the slower ^{15}N transverse relaxation during detection, the possibility for more efficient decoupling in both dimensions, and relaxation optimized properties of the pulse sequences. As a result, the median S/N in the ^{15}N observe CAN experiment is 16% higher than in the ^{13}C observe NCA-DIPAP experiment. In addition, significantly higher sensitivity was observed for those residues that are hard to detect in the NCA-DIPAP experiment, such as Gly, Ser and residues with high-field C^{α} resonances. Both CAN and CON experiments are able to detect Pro resonances that would not be observed in conventional proton-detected experiments. In addition, those experiments are free from problems of incomplete deuterium-to-proton back exchange in amide positions of perdeuterated proteins expressed in D_2O. Thus, these features and the superior resolution of ^{15}N-detected experiments provide an attractive alternative for main chain assignments. The experiments are demonstrated with the small model protein GB1 at conditions simulating a 150 kDa protein, and the 52 kDa glutathione S-transferase dimer, GST.

Keywords ^{15}N direct detection · CAN · CON · HSQC · Nuclear magnetic resonance (NMR) · Resonance assignment

Electronic supplementary material The online version of this article (doi:10.1007/s10858-010-9430-z) contains supplementary material, which is available to authorized users.

K. Takeuchi · G. Heffron · Z.-Y. J. Sun · D. P. Frueh · G. Wagner (✉)
Department of Biochemistry and Molecular Pharmacology, Harvard Medical School, 240 Longwood Avenue, Boston, MA 02115, USA
e-mail: gerhard_wagner@hms.harvard.edu

D. P. Frueh
Department of Biophysics and Biophysical Chemistry, Johns Hopkins University School of Medicine, Baltimore, MD 21205, USA

K. Takeuchi
Biomedicinal Information Research Center, National Institute of Advanced Industrial Science and Technology, Tokyo 135-0064, Japan

Introduction

Heteronuclear direct-detection experiments, which take advantage of the slower relaxation properties of nuclei with a lower gyromagnetic ratio, γ, have recently been considered as tools for extending the limits of NMR in structural and functional studies of proteins. A variety of pulse sequences have been developed for resonance assignments and structure analyses of proteins using ^{13}C-direct detection (Serber et al. 2001; Arnesano et al. 2005; Lee et al.

2005; Bermel et al. 2003, 2006a, b; Takeuchi et al. 2008; Felli and Brutscher 2009; Hsu et al. 2009; Takeuchi et al. 2010). However, direct detection of ^{15}N, which has the lowest γ within nuclei located in the protein backbone, has not been extensively exploited so far. In the past, one-dimensional ^{15}N-direct detection experiments have been used to obtain structure information near active sites of paramagnetic proteins (Vance et al. 1997; Machonkin et al. 2004; Balayssac et al. 2006; John et al. 2006; Lin et al. 2009), but multidimensional experiments have not been developed. In addition, it was shown that the slow ^{15}N relaxation results in ultra high-resolution spectra, which is also quite attractive for diamagnetic proteins (Vasos et al. 2006).

Experiments that focus on ^{15}N detection have great promise for characterization of proline-rich sequences that are difficult to study with ^{1}H-detected experiments lacking the amide protons of the imino acids. Sequences of many prolines are often found in phosphorylation sites of regulatory domains of proteins that function in signaling pathways, in transcription factors or translational regulators. Little is known about structural changes due to phosphorylation.

Here, we present two ^{15}N direct-detection HSQC-type experiments. The CAN experiment provides sequential connections between ^{15}N resonances using $^{13}C^{\alpha}$ chemical shift matching (Fig. 1a). It correlates the amide nitrogen's of residue *i*, $^{15}N_i$, with those of the $^{13}C^{\alpha}$ spins in both the same residue ($^{13}C^{\alpha}_{i}$ and the proceeding one ($^{13}C^{\alpha}_{i-1}$, providing an alternative way for establishing assignment of main chain resonances using heteronuclear detection. This can be complemented with a ^{15}N detected CON experiment, which correlates the amide nitrogen's of residue *i*, $^{15}N_i$, to the $^{13}C'$ spin in the proceeding residue ($^{13}C'_{i-1}$ The combination of the two experiments yields assignment of backbone heavy atoms (^{15}N, $^{13}C^{\alpha}$, $^{13}C'$) including prolines. The feasibility of the experiments is demonstrated with the B1 domain of protein G at conditions simulating the tumbling of a 150 kDa protein, and the 52 kDa glutathione S-transferase dimer, GST.

Materials and methods

All chemicals were purchased from Sigma (St. Louis, MO) unless otherwise noted. All stable-isotope-labeled materials were acquired from Cambridge Isotope laboratories (Cambridge, MA).

Expression and purification of the B domain of protein G (GB1)

The gene for His_6-tagged GB1, consisting of 64 amino acid residues, was cloned into the pET9d vector (Novagen, San Diego, CA) as previously described (Frueh et al. 2005). GB1 was expressed in commercially available BL21 (DE3) *E. coli* cells (Novagen) at 37°C and protein expression was induced for 6 h at the same temperature. For uniformly $^{2}H^{15}N^{13}C$ labeled samples, the cells were cultured in ^{2}H, ^{15}N, ^{13}C M9 media containing 8.5 g/l Na_2HPO_4, 3 g/l KH_2PO_4, 0.5 g/l NaCl, 2 mM $MgCl_2$, 0.1 mM $CaCl_2$ in D_2O, which was supplemented with 2 g/l $^{2}H^{13}C$ glucose and 1 g/l of $^{15}NH_4Cl$. The protein was purified with Ni–NTA affinity chromatography as previously described (Frueh et al. 2005).

Expression and purification of the glutathione S-transferase

The commercially available pGEX-4T-1 vector (GE Healthcare Biosciences, Pittsburgh, PA) was used to express Glutathione S-Transferase (GST) protein. The pGEX-4T-1 vector expresses the 26-kDa GST protein with a 19 amino-acid residue C-terminal flexible tail, which contains a thrombin cleavage site. Uniformly $^{2}H^{15}N^{13}C$-labeled GST was expressed in commercially available BL21 (DE3) *E. coli* cells (Novagen) at 25°C and protein expression was induced for 12 h. Culture media for the expression were the same as for uniformly $^{2}H^{15}N^{13}C$-labeled GB1. The protein was purified with Glutathione Sepharose affinity chromatography (GE Healthcare Biosciences) following manufacturer's recommendation. The C-terminal flexible tail was cleaved by Thrombin and the resultant 226 amino-acids GST protein was purified by Superdex-75 gel filtration column as a 52 kDa homodimer.

NMR experiments for GB1

NMR spectra were recorded on a Bruker (Billerica, MA) Avance 500 spectrometer equipped with a triple-resonance cryogenic probe (TXO) equipped with the carbon/nitrogen inner coil and cryogenic preamps, designed for heteronuclear-detection experiments. Spectra of the uniformly $^{2}H^{15}N^{13}C$-labeled GB1 sample (4 mM) were recorded at 8°C in buffer containing 10 mM sodium phosphate (pH 6.8), 100 mM NaCl, 20% w/v deuterated glycerol in D_2O with 3 mM Gd (DTPA-BMA). The molecular tumbling of GB1 under those conditions corresponds to a 150 kDa protein at 25°C (Takeuchi et al. 2008). The 2D CAN experiments were recorded with spectral widths of 1,721 (^{15}N, direct) and 3,769 Hz (^{13}C, indirect). The two-dimensional NCA experiments, with a double IPAP (DIPAP) scheme (Bermel et al. 2006b), were recorded with spectral widths of 3,754 (^{13}C, direct) and 1,722 Hz (^{15}N, indirect). In both spectra, ^{13}C and ^{15}N frequencies were centered at 55 and 117 ppm, respectively. For the 2D CAN experiment, 1,232 (^{15}N, direct dimension) and 100 (^{13}C, indirect dimension) complex data points were recorded. In the 2D NCA-DIPAP experiment,

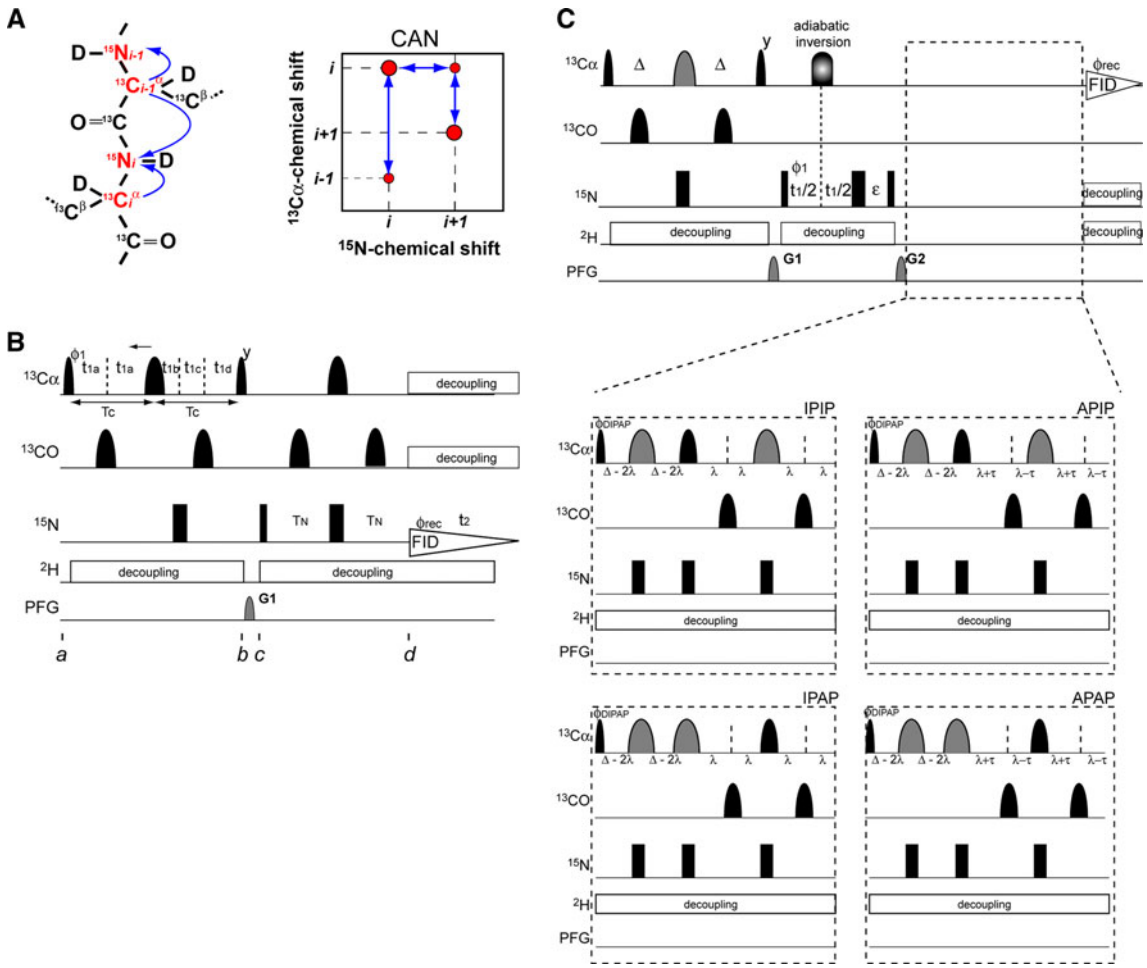

Fig. 1 Design and pulse scheme of the CAN experiment optimized for uniformly $^{2}H^{15}N^{13}C$-labeled samples. **a** Illustration of the coherences correlated in the CAN experiment with a schematic representation of the 2D CAN spectrum. The nuclei involved in this experiment are colored in *red*. *Arrows* indicate the magnetic transfer pathways in the CAN experiment. **b** and **c** Pulse program of **b** the nitrogen-detected CAN experiment and **c** the carbon-detected 2D NCA-DIPAP experiment (Bermel et al. 2006b). Narrow and wide black bars indicate nitrogen $\pi/2$ and π pulses, respectively. Narrow and wide semi elliptical shapes on the carbon channel represent $\pi/2$ and π Gaussian cascades pulses selective for the frequencies of aliphatic carbon nuclei (Q5/256 and Q3/205 μs, respectively) (Emsley and Bodenhausen 1992). Wider Gaussian shapes in gray indicate C^{α} selective Gaussian cascades pulses (Q3/1,557 μs). In the CAN experiment, carbon decoupling during the nitrogen-detection period was achieved by using WURST broadband adiabatic inversion (Kupče and Freeman 1995; Kupče et al. 1996). Broadband adiabatic inversion was also used for the carbon decoupling during nitrogen evolution in the NCA-DIPAP experiment. All pulses are applied along the x-axis unless otherwise indicated. The short delay $\varepsilon = 5$ μs compensates for the non-zero value of the initial t_1 increment. The phase cycle employed was $\phi_1 = (x, -x)$, $\phi_{rec} = (x, -x)$ for the CAN experiment. For the NCA experiment $\phi_1 = (x, -x)$, $\phi_{DIPAP} = (x, x, x, x, -x, -x, -x, -x)$ for IPIP and APAP, $(-y, -y, -y, -y, y, y, y, y)$ for APIP, and $(y, y, y, y, -y, -y, -y, -y)$ for IPAP, $\phi_{rec} = (x, -x, -x, x, -x, x, x, -x)$. Phase sensitive spectra in the indirect dimension are obtained by incrementing the phases ϕ_1 in a States-TPPI manner (Marion et al. 1989). The recycling delay is optimized based on the longitudinal relaxation rate of the excited nucleus. The sine-shaped pulsed field gradients were applied along the z-axis for 1.0 ms with maximum intensities of G1 = 10 G/cm for the CAN experiment and G1 = 15 G/cm and G2 = 25 G/cm for the NCA-DIPAP experiment. Deuterium and nitrogen decoupling are achieved by using WALTZ16 (1 kHz) (Shaka et al. 1983) and GARP (Shaka et al. 1985; 1.5 kHz), respectively

1,360 (^{13}C, direct) and 100 (^{15}N, indirect) complex data points were recorded. For each increment, 160 scans were accumulated. For reconstructing the ^{13}C-decoupled data from the DIPAP scheme, 53.8 Hz $^{1}J_{C\alpha C\beta}$ and 34.5 Hz $^{1}J_{C\alpha C'}$ couplings were used, which are the default values in TOPSPIN (Bruker; Billerica, MA). A cosine-apodization function was applied for each FID and zero filled to 2,048 data points in the direct dimension before Fourier transformation. For the indirect dimensions, a cosine-apodization function and zero fill to 256 data points were applied. The digital resolution in the direct and indirect dimensions after Fourier transformation was 0.87 and 15 Hz for the 2D CAN experiment and 1.8 and 6.7 Hz for the 2D NCA experiment. The recycling delay was set to 1.6 s for both experiments. All

spectra were processed with TOPSPIN or XWINNMR (Bruker; Billerica, MA) and analyzed with the program Sparky (Goddard and Kneller 2004).

NMR experiments for GST

NMR spectra were recorded on the same instrument as the GB1 sample. Spectra of the uniformly $^{2}H^{15}N^{13}C$-labeled GST dimer (0.75 mM, 1.5 mM as monomer concentration) were recorded at 25°C in a buffer containing 10 mM sodium phosphate (pH 6.8), 100 mM NaCl, and 4 mM Gd (DTPA-BMA) in D_2O. The 2D CAN experiments were recorded with spectral widths of 2,541 (^{15}N, direct) and 3,769 Hz (^{13}C, indirect) with the center frequencies at 122 ppm (^{15}N) and 55 ppm (^{13}C), respectively. 512 (direct) and 105 (indirect) complex data points were recorded. For each increment, 768 scans were accumulated. The 2D CON experiment was recorded with spectral widths of 2,541 (^{15}N, direct) and 2,513 Hz (^{13}C, indirect) with the center frequencies at 122 ppm (^{15}N) and 176 ppm (^{13}C), respectively. 512 (direct) and 41 (indirect) complexed data points were recorded with $Tc = 8.5$ ms and $\Delta = 14.5$ ms. For each increment, 672 scans were accumulated. The 3D TROSY-HNCA experiment was recorded after exchanging the media from D_2O to H_2O. The sample was left at room temperature for 4 days to promote D to H exchange in amide positions. The experiment was recorded with a spectral width of 9,615 (direct) × 2,675 (indirect, N) × 4,829 Hz (indirect, ^{13}C) with the center frequencies at 4.7 ppm (^{1}H), 120 ppm (^{15}N) and 55 ppm (^{13}C). 512 (direct) × 32 (indirect, N) × 64 (indirect, ^{13}C) complex data points were recorded. For each increment, 24 scans were accumulated. For all GST spectra, a cosine-apodization function was applied for each FID, then zero filled up to 1,024 data points for the direct dimension before Fourier transform. The recycling delay was set to 1.8 s. 2D CAN, CON, and 3D TROSY-HNCA were recorded for 3.5, 1.5 and 3 days, respectively. All spectra were processed with TOPSPIN or XWINNMR (Bruker; Billerica, MA) and analyzed with the program Sparky (Goddard and Kneller 2004).

Experimental design

In principle, the CAN nitrogen-detected experiment provides the same correlations as the ^{13}C-detected NCA experiment (Bermel et al. 2006b; Takeuchi et al. 2008). In practice, it may provide additional resolution in the nitrogen dimension and it can be achieved with a simpler pulse sequence resulting in a comparable but more uniform sensitivity. In a rough estimate, the intensity of a signal is proportional to γ of the excited nucleus and to $\gamma^{3/2}$ of the detected nucleus (Ernst 1987). Since $(\gamma_N/\gamma_C)^{3/2}$ is 0.25, the intensities of detected ^{15}N nuclei are expected to be four times lower than those of detected ^{13}C nuclei, assuming equal polarization. However, $^{13}C^{\alpha}$ direct detection of a uniformly ^{13}C-labeled protein is not straightforward owing to the presence of several strong one-bond ^{13}C–^{13}C couplings that split the signals into multiplets and hence reduce the sensitivity. While the spectral complexity can be avoided by computational deconvolution (Shimba et al. 2003), spin-state selective schemes such as IPAP (Bermel et al. 2007), or a recently developed ^{13}C–^{12}C alternate labeling strategy (Takeuchi et al. 2008), using a ^{15}N direct-detection experiment is a good alternative to avoid this problem. Since ^{13}C evolution is performed in the indirect dimension, evolutions under multiple ^{13}C–^{13}C scalar couplings can easily be refocused by the application of inversion pulses and by using a constant-time periods. In addition, since the height of a detected signal is given by the integral over the envelope of the detected signal, sensitivity losses due to the lower γ of ^{15}N nuclei can at least partially be compensated by the slower transverse relaxation of ^{15}N.

Figure 1b shows the pulse scheme of the CAN nitrogen-detected experiment for a uniformly $^{2}H^{15}N^{13}C$-labeled sample. The first INEPT module converts a carbon C_i^{α} single quantum coherence (SQC) into longitudinal two-spin order involving C_i^{α} and either of the two scalar-coupled nitrogen's (N_i and N_{i+1}) (b). Concomitantly, the coherence is encoded with the C_i^{α} chemical shift in either a semi-constant time (SCT; Grzesiek and Bax 1993; Logan et al. 1993) or a constant-time fashion, depending on the value of n_{1max}. The density operator, σ, at point b is thus:

$$\sigma_b = \cos\left((\omega_{C_i^{\alpha}})t_1\right)\left(2N_{zi}C_z^{\alpha}S_C(^{1}J_{i/i})C_C(^{2}J_{i/i+1}) + 2N_{zi+1}C_z^{\alpha}iS_C(^{2}J_{i/i+1})C_C(^{1}J_{i/i}) + \ldots\right)e^{-2T_c/T_{2C\alpha}} \quad (1)$$

where only the real component of the indirect FID is depicted. $S_C(^{1}J_{i/i}) = sin(\pi^{1}J_{CaiNi}2T_C)$ and $S_C(^{2}J_{i/i+1}) = sin(\pi^{2}J_{CaiNi+1}2T_C)$, while C stands for a *cosine* of the corresponding arguments. $T_{2C\alpha}$ is the transverse relaxation rate for $^{13}C^{\alpha}$. The initial value of the SCT/CT period $2T_C$ is set to $1/^{1}J_{C\alpha C\beta}$ (28 ms) to minimize losses due to scalar couplings between $^{13}C^{\alpha}$ and $^{13}C^{\beta}$. The tuning of the delay is also set to minimize evolution into doubly antiphase coherences involving both neighboring nitrogen's, which would end up in non-detectable double quantum coherence. The evolution in t_1 under this coupling is scaled from $1/SW_C$ to $1/SW_C - 2T_C/n_{max}$ in the SCT evolution and null in the CT evolution. The following module (*c*-*d*) converts nitrogen antiphase SQCs into detectable N^{H} single quantum coherences:

$$\sigma_d = \cos\left((\omega_{C_i^{\alpha}})t_1\right) \times \begin{pmatrix} N_{yi}S_C(^1J_{i/i})C_C(^2J_{i/i+1})S_N(^1J_{i/i})C_N(^2J_{i-1/i})e^{-i\omega i+t2}+ \\ N_{yi+1}S_C(^2J_{i/i+1})C_C(^1J_{i/i})S_N(^2J_{i/i+1})C_N(^1J_{i+1/i+1})e^{-i\omega i+t2}+\ldots \end{pmatrix} e^{-2T_C/T_{2C\alpha}}\, e^{-2T_N/T_{2N}} \quad (2)$$

where $S_N(^1J_{i/i}) = sin(\pi^1 J_{CaiNi} 2T_N)$ and $S_N(^2J_{i/i+1}) = sin(\pi^2 J_{CaiNi+1} 2T_N)$, while C stands for a *cosine* of the corresponding arguments. T_{2N} is the transverse relaxation rate for $^{15}N_H$. To maximize the amplitude of both intra-residual and sequential coherences, $2T_N$ is set to $1/4J_{C\alpha N}$ ($\sim$22 ms). Note that sequential coherences reach their maximum at $\sim$70 ms unless T_{2N} is longer than 60 ms, however, the intra-residual correlations are largely suppressed in this case. See Fig. S1 for the evolution of the N single quantum coherences in the CAN experiment. Compared to the NCA double IPAP (NCA-DIPAP) experiment (Fig. 1c), the carbon transverse period of the CAN experiment is significantly shorter (28 ms in CAN compared to 44 ms in NCA-DIPAP). Instead, the CAN experiment has 22 ms of a slower-relaxing nitrogen-transverse period. Thus, in the CAN experiment, signal losses due to relaxation of coherences during the pulse sequence are significantly less than in the NCA-DIPAP experiment. This ameliorates the intrinsic low sensitivity of the CAN experiment.

Instead of the "out-and-stay" type transfer used in this paper, one can also consider a "out-and-back" CAN experiment, which utilizes ^{15}N nuclei for both excitation and detection. Although, the carbon transverse period can be minimized in this way, excitation of the lower γ nuclei decreases the sensitivity further by 2.5-fold. In addition, a longer longitudinal-relaxation time of ^{15}N nuclei would require a longer repetition delay, which would decrease the time-efficiency of the experiment. Thus, the "out-and-stay" sequence that excites higher γ ^{13}C nuclei while taking advantage of the slower transverse relaxation of ^{15}N nuclei for detection is preferred.

Result and discussion

Experiments were recorded on a 4 mM sample of the B1 domain of protein G (GB1) uniformly $^2H^{15}N^{13}C$-labeled and dissolved in D_2O buffer supplemented with 3 mM Gd (DTPA-BMA). To simulate the tumbling of a 150 kDa protein, 20% glycerol was added, and the experiment was recorded at 281 K [for a calibration of the correlation time, see (Takeuchi et al. 2008)]. All experiments were recorded in D_2O to minimize the proton-nitrogen and proton-carbon dipole interactions between H_N and $^{15}N_H$ or $^{13}C^{\alpha}$. Paramagnetic reagents, such as Gd(DTPA-BMA) or Ni(DO2A) have been used for efficient detection of carbon and proton resonance without significantly accelerating transverse relaxation rates (Eletsky et al. 2003; Cai et al. 2006; Takeuchi et al. 2010). Addition of 3 mM Gd (DTPA-BMA) to the "150 kDa" GB1 sample decreased T_1 values for C^{α} from 4.3 to 1.3 s. The average transverse relaxation times, T_2, of $^{13}C^{\alpha}$ and ^{15}N estimated from a spin echo experiment was 60 ms for $^{13}C^{\alpha}$ and 120 ms for ^{15}N after addition of 3 mM Gd (DTPA-BMA). Since the T_2 of $^{13}C^{\alpha}$ and ^{15}N were 70 and 140 ms, respectively, before addition of the paramagnetic relaxation agents, only a $\sim$14% decrease in T_2 is observed. Thus, it becomes possible to accumulate scans $\sim$3.3 times as fast in presence of the relaxation agent. This, in turn represents a $\sim$1.8 fold gain in S/N.

Figure 2a shows the comparison between the nitrogen-detected 2D CAN spectrum and the carbon-detected 2D NCA-DIPAP spectrum. The measuring time for each spectrum was 15 h. Both spectra are shown with the same scale in Hz for the direct dimension and the same number of points was recorded for the indirect dimension. The acquisition time for the direct dimension was set to approximately $3 \times T_2$ of the detected nuclei of each experiment (358 ms for CAN and 181 ms for NCA-DIPAP), so that a sufficient resolution is achieved without significantly sacrificing sensitivity (Rovnyak et al. 2004). A cosine-apodization function was applied to suppress the artifacts due to time-domain signal truncation, and each FID was zero filled up to 2,048 data points before Fourier transform. The digital resolution for the direct dimensions after Fourier transformation was 0.84 and 1.8 Hz for the CAN and NCA-DIPAP experiment, respectively.

Comparison of slices for the same correlation (Phe52 intra-residual cross peak, marked with an asterisk at the top traces of the Fig. 2a and b, and in the enlarged insert panels) demonstrates that the line-width in the direct dimension is much narrower in CAN than in NCA. The line width for the intra-residual correlation peak of Phe52 (without apodization) was 3.4 Hz for CAN and 11 Hz for NCA-DIPAP. Whereas the line width (LW) for nitrogen is almost comparable to the value estimated from T_2 ($LW = 1/T_2 \times 1/\pi = 2.7$ Hz), the LW for carbon was much broader than the estimated value ($LW_{RX} = 5.3$ Hz). This emphasizes the difficulty of achieving a perfect decoupling in the DIPAP scheme. In contrast to the NCA experiment (see below), all intra-residual as well as sequential correlations were observed in the nitrogen-detected CAN experiment (See Fig. S2 for CAN spectrum with assignment procedures). It is

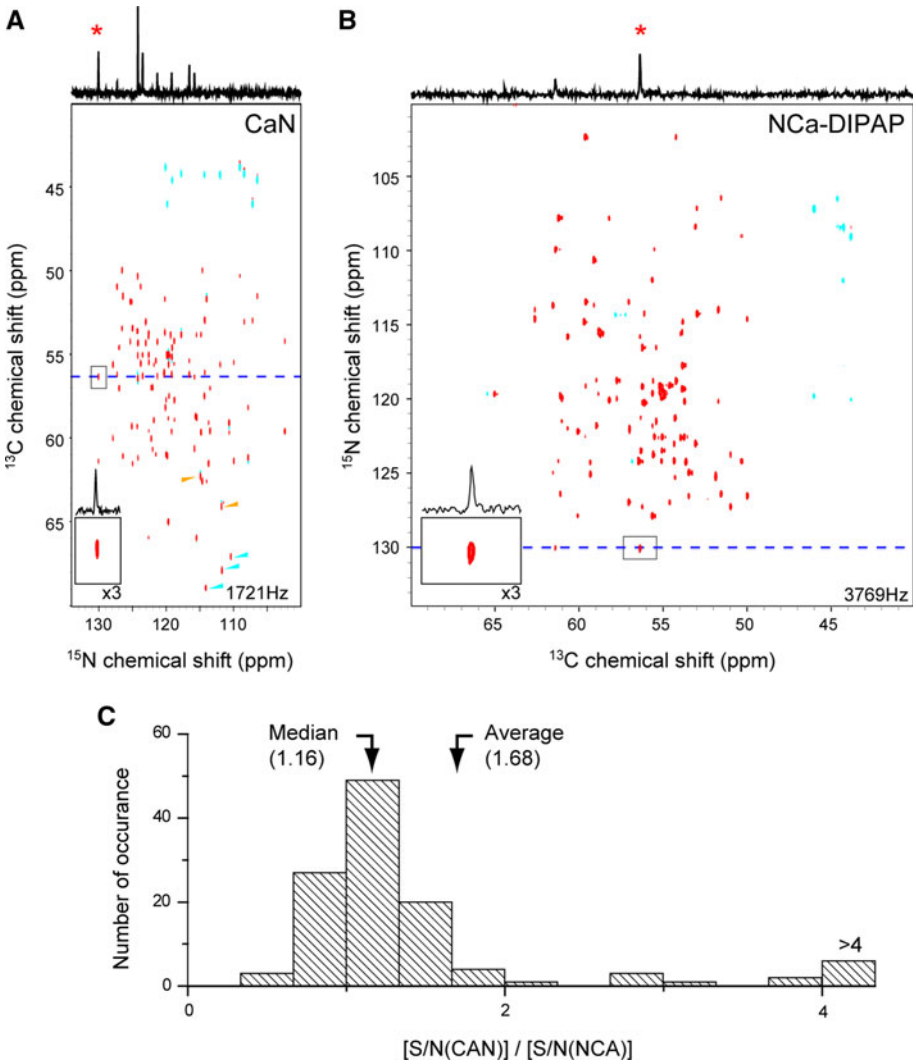

Fig. 2 Comparison of the CAN experiment with the NCA-DIPAP experiment. **a** CAN and **b** NCA-DIPAP spectra of uniformly $^{2}H^{15}N^{13}C$ labeled GB1 (4 mM) recorded at conditions simulating a 150 kDa protein (20% glycerol, 281 K). The measurement times for the CAN and NCA-DIPAP experiments were 15 h, each. Both spectra are shown at the same scale in Hz for the direct dimension and the same number of points was recorded for the indirect dimension. Positive and negative correlation peaks are shown in *red* and cyan, respectively. The Phe52 intra-residual cross peak is enlarged in the insert panels and the corresponding one-dimensional slices along the direct dimension are shown at the top of the 2D spectrum as well as in the enlarged panels. In the 2D CAN spectrum, *cyan* and *orange arrowheads* indicate side chain correlations from Asn (C^{β}-N^{δ}) and Gln (C^{γ}-N^{ε}), respectively. The 2D CAN experiment was recorded with a spectral width of 1,721 (direct) × 3,769 Hz (indirect). The NCA-DIPAP experiment was recorded with a spectral width of 3,754 (direct) × 1,722 Hz (indirect). In both spectra, ^{13}C and ^{15}N frequencies were centered at 55 and 117 ppm, respectively. For the 2D CAN spectrum, 1,232 (direct) × 100 (indirect) complexed data points were recorded with $Tc = 14$ ms and $T_N = 11$ ms. Whereas 1,360 (direct) × 100 (indirect) complex data points with $Tc = 11$ ms were recorded for the 2D NCA-DIPAP experiment. For each increment, 160 scans were acquired. For the reconstruction of the decoupled data from the DIPAP scheme, 53.8 Hz $^{1}J_{C\alpha C\beta}$ and 34.5 Hz $^{1}J_{C\alpha C'}$ couplings were used. Those are the default values in the software TOPSPIN (Bruker; Billerica, MA). A cosine apodization function was applied to each FID, and the direct dimensions were zero-filled up to 2,048 data points before Fourier transform. **c** Histogram of the S/N ratios in the CAN versus the NCA-DIPAP experiment. The right most column is for all correlations that showed [S/N(CAN)]/[S/N(NCA-DIPAP)] > 4

interesting to note that the side chain correlations from Asn (C^{β}-N^{δ}) and Gln (C^{γ}-N^{ε}) were also observed in the 2D CAN spectrum (cyan and orange arrowheads, respectively in Fig. 2a).

In the NCA-DIPAP experiment, one intra-residue (Thr25 C^{α}-N) and two sequential (Thr25 C^{α}-Ala26 N, and Ser58 C^{α}-His59 N) correlations were not observed. This is due to the application of selective C^{α} pulses in the DIPAP scheme and results from imperfect inversions of high-field C^{α} resonances. As the Phe52 intra-residual cross peak showed almost the same S/N in the CAN and NCA-DIPAP experiments, it seems that the lower γ of ^{15}N nuclei was fully

compensated by the slower ^{15}N transverse relaxation rate, a better decoupling scheme for the detected nuclei, as well as the relaxation-optimized properties of the pulse sequence.

This is clearly summarized in Fig. 2c, as the median of the S/N in the CAN experiment is 16% higher than that of the NCA-DIPAP experiment. The average of the S/N was even higher for the nitrogen-detected experiment ([*S/N (CAN)*]/[*S/N (NCA-DIPAP)*] = 1.69) since Gly, Ser and some high-field C^{α} signals are significantly weaker in the NCA-DIPAP experiment. There are 12 correlations that have >2.5 times better S/N in the CAN experiment compared to the NCA-DIPAP experiment. These correlations originate from Gly (4/5 residues) and Ser (1/1 residue) as well as one of the Thr signals that showed a significantly high-field C^{α} chemical shift (66.0 ppm). No signal in the CAN experiment was below 50% of the corresponding NCA-DIPAP signal.

As discussed above, sequential coherences reach their maximum at $2T_N \sim 70$ ms, when the intra-residual correlations are largely suppressed. Figure 3 shows a comparison of the nitrogen-detected 2D CAN spectrum with $2T_N = 22$ ms (A, C) and 70 ms (B, D). It is clearly shown that the intra-residual correlations are suppressed with a 70 ms delay, whereas, sequential coherences have in average a S/N that is 16% higher at 70 ms than at 22 ms (Fig. 3e).

While the 2D spectra shown here are well dispersed with narrow lines and exhibit good sensitivity, the sensitivity and resolution can be further improved by using non-uniform sampling with suitable processing schemes (Hyberts et al. 2010). As shown in supplemental Fig. S3, a comparable spectrum was obtained with non-uniform sampling and FM reconstruction. The sampling schedule was designed by selecting gaps according to a Poisson distribution (Hyberts et al. 2010). The measuring time was 6.5 h compared to the 15 h needed with uniform sampling. With the exception of two sequential correlations (Thr18 $^{13}C^{\alpha}$- Glu19 $^{15}N_H$ and Thr49 $^{13}C^{\alpha}$- Lys50 $^{15}N_H$), all intra-residue and sequential correlations are observed in the non-uniformly sampled CAN spectrum.

Alternate ^{13}C–^{12}C labeling may also be used in conjunction with the CAN experiment. There are two benefits associated with alternate ^{13}C–^{12}C labeling. Due to the absence of the $^{1}J_{C\alpha C\beta}$ coupling, the carbon–nitrogen INEPT delay (*a-b*, in Fig. 1) can be shortened from 28 to 22 ms (the optimal value depends also on the $^{13}C^{\alpha}$ T_2), which reduces sensitivity losses during this period. For instance the 52 kDa GST dimer, which we will discuss below, has a $^{13}C^{\alpha}$ T_2 of 30 ms. In this case, we estimate that about 30% stronger coherences will be preserved in the first INEPT transfer.

Furthermore, if the neighboring residues are not ^{13}C labeled in the C^{α} position, the conversion of nitrogen antiphase SQCs into the detected N^H single quantum coherences becomes more efficient. For this case, the evolution of the intra-residual correlation in uniformly ^{13}C-labeled protein can be modified from (2) to the following:

$$\sigma_d = \cos\left((\omega_{C_i^{\alpha}})t_1\right) \times \begin{pmatrix} N_{yi}S_C(^1J_{i/i})C_C(^2J_{i/i+1})S_N(^1J_{i/i})C_N(^2J_{i-1/i})e^{-i\omega it2} \\ -2N_{xi}C^{\alpha}_{z}iS_C(^1J_{i/i})C_C(^2J_{i/i+1})C_N(^1J_{i/i})S_N(^2J_{i-1/i})e^{-i\omega it2} \end{pmatrix} e^{-2T_C/T_{2C\alpha}}\, e^{-2T_N/T_{2N}} \tag{2-1}$$

If C^{α} of residue $i-1$ is not ^{13}C labeled, $S_N(^2J_{i-1/i})$ becomes zero and $C_N(^2J_{i-1/i})$ becomes one, since there is no $^2J_{i-1/i}$ coupling. Thus, only the detectable term of Eq. (2-1) would remain, avoiding the leakage of coherence to undetectable term, and the expression simplifies to:

$$\sigma_d = \cos\left((\omega_{C_i^{\alpha}})t_1\right) \times N_{yi}S_C(^1J_{i/i})C_C(^2J_{i/i+1})S_N(^1J_{i/i})e^{-i\omega it2}\, e^{-2T_C/T_{2C\alpha}}\, e^{-2T_N/T_{2N}} \tag{3-1}$$

Similarly, the sequential correlation in uniformly ^{13}C-labeled protein can be re-written in a modified form of Eq. (2), (2-2), including a non-detectable term.

$$\sigma_d = \cos\left((\omega_{C_i^{\alpha}})t_1\right) \times \begin{pmatrix} N_{yi+1}S_C(^2J_{i/i+1})C_C(^1J_{i/i})S_N(^2J_{i/i+1})C_N(^1J_{i+1/i+1})e^{-i\omega i+1t2} \\ -2N_{zi+1}C^{\alpha}_{z}iS_C(^2J_{i/i+1})C_C(^1J_{i/i})C_N(^2J_{i/i+1})S_N(^1J_{i+1/i+1})e^{-i\omega i+1t2} \end{pmatrix} e^{-2T_C/T_{2C\alpha}}\, e^{-2T_N/T_{2N}} \tag{2-2}$$

If C^{α} of residue $i + 1$ is not ^{13}C labeled, $S_N(^2J_{i+1/i+1})$ becomes zero and $C_N(^2J_{i+1/i+1})$ becomes one, since there is no coupling value for $^1J_{i+1/i+1}$. Thus, only the detectable term of Eq. (2-2) would remain, avoiding the leakage of coherence to undetectable terms Eq. (3-2).

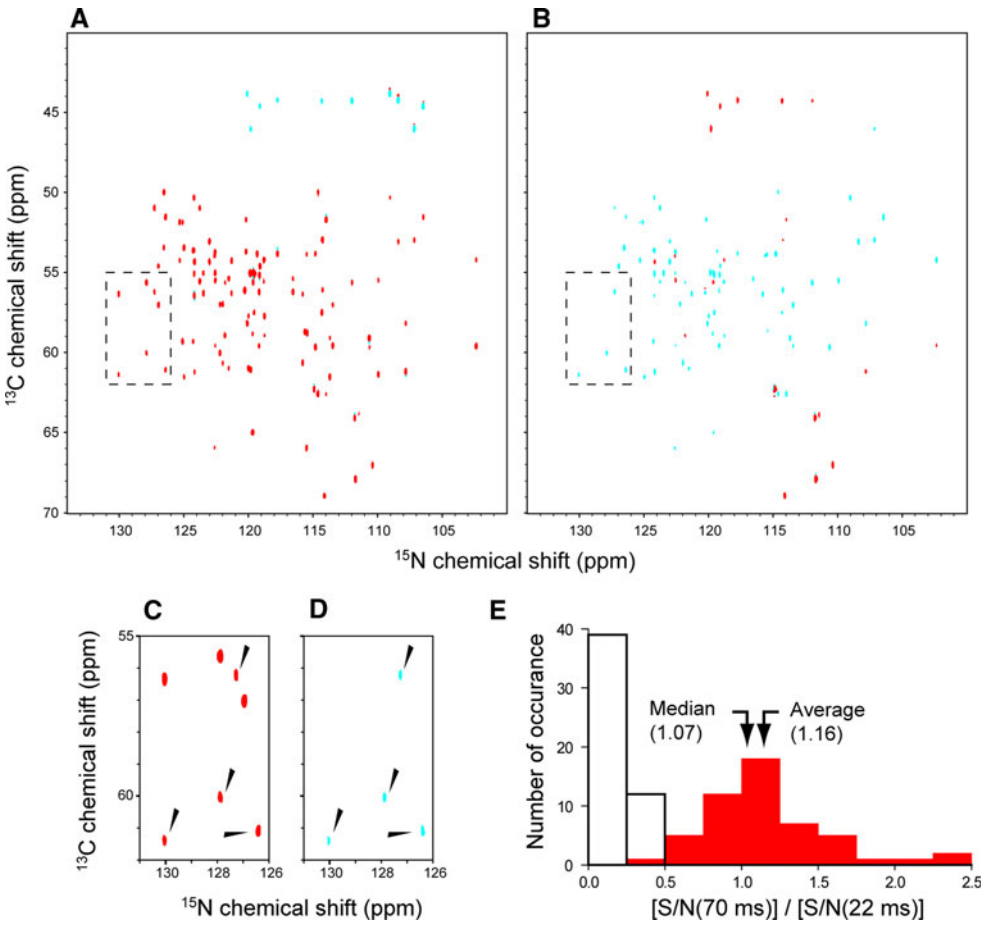

Fig. 3 Comparison of the CAN experiment recorded with different nitrogen refocusing periods (T_N). **a** The CAN spectrum of uniformly $^{2}H^{15}N^{13}C$ labeled GB1 (4 mM) recorded with the same conditions as in Fig. 2, with $T_N = 11$ ms. **b** same with $T_N = 35$ ms. *Positive* and negative correlation peaks are shown in red and cyan, respectively. The regions boxed in (**a**) and (**b**) are enlarged in (**c**) and (**d**). The measuring time for both spectra were 15 h, each. In the enlarged 2D CAN spectra, *black arrowheads* indicate sequential correlations. **e** Histogram of the ratios of S/N in the CAN experiment with $T_N = 35$ and 11 ms. Sequential and intra-residual correlations are shown with solid red and open black bars, respectively

$$\sigma_d = \cos\left((\omega_{C_i^\alpha})t_1\right) \times N_{yi+1}S_C(^2J_{i/i+1})C_C(^1J_{i/i})S_N(^2J_{i/i+1})e^{-i\omega i+1t2}\, e^{-2T_C/T_{2C\alpha}}\, e^{-2T_N/T_{2N}} \tag{3-2}$$

More generally, if the C^α ^{13}C labeling ratio of residue $i-1$ and $i+1$ is written as L_{i-1} and L_{i+1}, respectively. Equation 3-1 and 3-2 are written as:

$$\sigma_d = \cos\left((\omega_{C_i^\alpha})t_1\right) \times \begin{pmatrix} N_{yi}S_C(^1J_{i/i})C_C(^2J_{i/i+1})S_N(^1J_{i/i})C_N(^2J_{i-1/i})e^{-i\omega it2} \times L_{i-1} + \\ N_{yi}S_C(^1J_{i/i})C_C(^2J_{i/i+1})S_N(^1J_{i/i})e^{-i\omega it2} \times (1 - L_{i-1}) + \ldots \end{pmatrix} e^{-2T_C/T_{2C\alpha}}\, e^{-2T_N/T_{2N}} \tag{4-1}$$

And

$$\sigma_d = \cos\left((\omega_{C_i^\alpha})t_1\right) \times \begin{pmatrix} N_{yi+1}S_C(^2J_{i/i+1})C_C(^1J_{i/i})S_N(^2J_{i/i+1})C_N(^1J_{i+1/i+1})e^{-i\omega i+1t2} \times L_{i+1} + \\ N_{yi+1}S_C(^2J_{i/i+1})C_C(^1J_{i/i})S_N(^2J_{i/i+1})e^{-i\omega i+1t2} \times (1 - L_{i+1}) + \ldots \end{pmatrix} e^{-2T_C/T_{2C\alpha}}\, e^{-2T_N/T_{2N}} \tag{4-2}$$

Supplemental Fig. S4 shows the evolution of the intra-residual and sequential correlations with different $^{13}C^\alpha$ labeling ratios in the neighboring residues. Both intra-residual and sequential correlations are transferred more efficiently with lower $^{13}C^\alpha$-labeling ratios in the neighboring residues. It may be beneficial to use this strategy for

large molecular weight proteins to enhance the sensitivity of weaker sequential correlations. In the case of the GST dimer (80 ms nitrogen T_2 and 30 ms $^{13}C^{\alpha}$ T_2), a sequential correlation with <20% $^{13}C^{\alpha}$ labeling ratio in the succeeding residue is expected to be more than twice as sensitive as when using uniform ^{13}C labeling (22 ms nitrogen delay). The alternate ^{13}C–^{12}C labeling can also be used to classify the amino acid type of neighboring residues since different labeling patterns occur for different amino acids. Figure S5 shows the ratio of signal intensity for sequential correlations between the spectra recorded with 22 and 60 ms nitrogen refocusing periods. The ratio becomes negative for those residues that have a succeeding residue with 100% $^{13}C^{\alpha}$ labeling (Ala, Cys, Gly, His, Phe, Ser, Tyr, Trp, and Val), while other residues exhibit positive values. This information provides valuable hints about the amino-acid types of succeeding residues along with its chemical shift information.

We also recorded the 2D CAN experiment for the 52 kDa GST protein dimer. A 0.75 mM sample of the uniformly $^{2}H^{15}N^{13}C$-labeled GST dimer (1.5 mM monomer concentration) was prepared in buffered D_2O and supplemented with 4 mM Gd(DTPA-BMA). The addition of the 4 mM Gd(DTPA-BMA) shortened the $^{13}C^{\alpha}$ T_1 for the entire protein including the core. The average T_1 for $^{13}C^{\alpha}$ measured under this condition was 1.4 s, which is significantly shorter than the T_1 value without Gd (DTPA-BMA) ($\sim$3.6 s). No signals with T_1 values longer than 1.8 s were observed in an inversion recovery experiment. T_2 values of 30 ms for $^{13}C^{\alpha}$ and 80 ms for ^{15}N were measured under these conditions. The $^{13}C^{\alpha}$ T_1 without Gd (DTPA-BMA) was shorter in GST than for GB1 at the "150 kDa" condition, consistent with a shorter rotational correlation time (τ_C) (or smaller molecular weight) of the GST protein. However, T_2 values were significantly shorter in GST most likely due to the presence of partial aggregation and/or exchange broadening in the GST sample. In a 3.5 day experiment, we could observe $\sim$250 resolved signals, which correspond to $\sim$54% of the total expected resonances, including both inter- or intra-residue signals (Fig. 4). The observed resonances are reasonably narrow and well dispersed, indicating the applicability of the CAN experiment to higher molecular weight protein systems at moderate concentrations. It is worth noting that 13 out of 14 Pro C^{δ}-N correlations were observed and are placed in a dashed frame in Fig. 4. All of the Pro C^{δ}-N correlations except one ($\delta N = 136$ ppm) can be associated with the corresponding C^{α}-N cross peaks with carbon chemical shifts around 61–67 ppm. Three of them have additional signals in carbon chemical shifts below 60 ppm, which correspond to sequential correlations. This indicates that most of the intra-residual correlations are observed in this spectrum, while sequential correlations are barely above the noise level. This is further confirmed by the smaller number of correlation peaks in the CAN experiment with a 70 ms nitrogen refocusing delay T_N, which selects for sequential over intra-residual correlations (see Fig. S1 and discussion above, data not shown). Since the sequential correlations are expected to be three times less sensitive compared to intra-residual correlations, with the estimated T_2 values for $^{13}C^{\alpha}$ and ^{15}N, using longer measuring times will significantly enhance the performance of this experiment. We expect that this is best achieved at higher magnetic fields where the sensitivity is improved by an enhanced polarization. It is clear that further improvements need to be introduced at the hardware level as well as in data acquisition and processing to enable a routine use of this experiment for very large proteins. However, as we will discuss below, a similar number of peaks are missing in the HNCA experiment recorded in a comparable experimental time (3 days) and the ^{1}H-^{15}N TROSY HSQC spectra. Thus, the absence of these correlations is likely due to a large degree to exchange processes and lack of optimization of sample conditions and not only due to a low sensitivity of the nitrogen detected experiments.

An experiment for detecting $^{13}C'$-^{15}N correlations, CON, was designed with a similar pulse scheme as in Fig. 1 (Fig. S6). While the $^{13}C'$ transverse relaxation is faster compared to $^{13}C^{\alpha}$ in higher molecular weight proteins and at high magnetic-field, it may nevertheless be beneficial to utilize the efficient coherence transfer pathway. In addition, the "out-and-stay" type transfer used in the CON experiment shortens the C′ transverse period to 33 ms compared to 66 ms used in NCO-IPAP, which use the "out-and-back" coherence pathway. Thus, the CON experiment may be less susceptible to signal loss due to CSA at high molecular weight and high magnetic fields. Figure 4b shows the CON spectrum for the 52 kDa GST protein dimer recorded under the same conditions as used in Fig. 3. The spectrum was recorded over 1.5 days, and we observed $\sim$160 resolved signals, which correspond to $\sim$71% of the expected resonances.

The CAN/CON nitrogen-detected experiments are ideally suited for detecting proline resonances. This is a clear advantage over conventional proton-detected sequences, such as the HNCA or related experiments where prolines cause gaps in the assignments, in particular if there are two or more in a row. Moreover, the CAN/CON experiments can use the unique proline chemical shifts as amino acid type markers to facilitate sequential assignments. In addition, the nitrogen-detected experiments do not suffer from incomplete deuterium to proton back-exchange in perdeuterated proteins that have been expressed in D_2O. This is clearly exemplified in Fig. 4c. The CA-N correlations observed in the CAN spectrum appear at nearly identical positions as in the TROSY-HNCA spectra. However, there

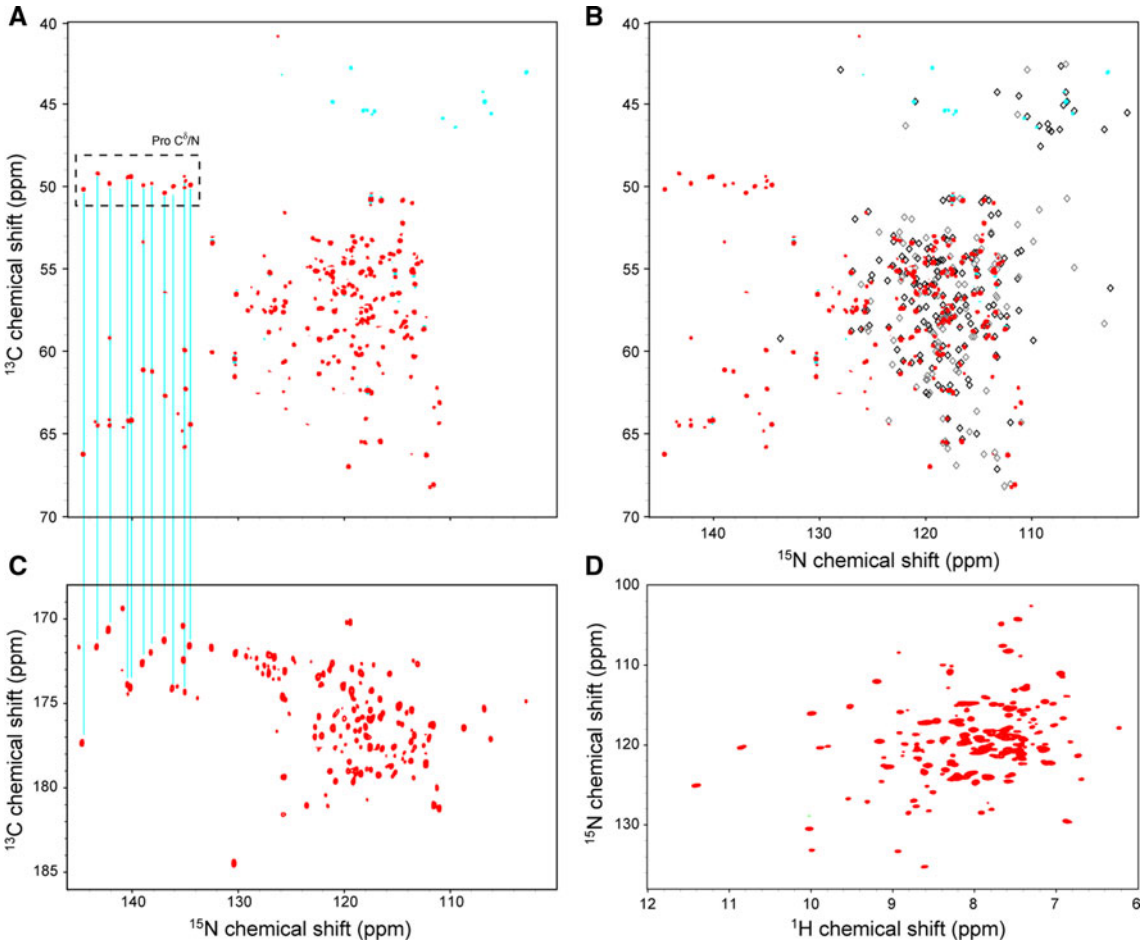

Fig. 4 **a** CAN and **b** CON spectra of uniformly $^{2}H^{15}N^{13}C$ labeled GST dimer (0.75, 1.5 mM monomer concentration) recorded at 298 K in buffered $^{2}H_2O$ supplemented with 4 mM Gd (DTPA-BMA). The CON experiment is described in the supporting information. *Positive* and *negative* correlation peaks are shown in *red* and *cyan*, respectively. **a** The *dashed rectangle* contains the proline C^{δ}-N correlations (*top left*). The proline C^{α}-N correlations are connected to C′-N correlations as well as C′-N correlations in (**b**) by cyan lines. The 2D CAN experiment was recorded with a spectral width of 2,541 (*direct*) × 3,769 Hz (*indirect*) with the center frequencies at 122 ppm (^{15}N) and 55 ppm (^{13}C). 512 (*direct*) × 105 (indirect) complexed data points were recorded with $Tc = 14$ ms and $T_N = 11$ ms. For each increment, 768 scans were accumulated. A cosine-apodization function was applied to each FID, which was followed by zero filling up to 1,024 data points for the direct dimension before Fourier transform. The recycling delay was set to 1.8 s. **b** The 2D CON experiment was recorded with spectral widths of 2,541 (*direct*) × 2,513 Hz (*indirect*) with the center frequencies at 122 ppm (^{15}N) and 176 ppm (^{13}C). 512 (*direct*) × 41 (*indirect*) complex data points were recorded with $Tc = 8.5$ ms and $T_N = 14.5$ ms (See Fig. S5 for the CON pulse scheme). For each increment, 672 scans were accumulated. A cosine-apodization function was applied to each FID, which was followed by zero filling up to 1,024 data points in the direct dimension. The recycling delay was set to 1.8 s. **c** The CAN spectrum shown in **a** is overlaid by the CAN correlations observed in a TROSY-HNCA spectrum recorded within the same experimental time, on a sample with the same concentration but dissolved in buffered H_2O. *Diamonds* in the spectrum indicate the position of the CAN correlations observed in the TROSY-HNCA spectrum. In cases where two C^{α} correlations are observed for one H–N pair, the stronger signal is shown in *black* while the weaker signal is indicated in gray. **d** ^{15}N-^{1}H TROSY spectrum of the uniformly $^{2}H^{15}N^{13}C$-labeled GST (1.5 mM monomer concentration), recorded at 289 K with a 600-MHz AVANCE spectrometer (Bruker) equipped with a cryogenic probe designed for proton-detected experiments. The experiment was recorded with spectral widths of 9,600 (*direct*) × 2,400 Hz (*indirect*) with ^{1}H and ^{15}N center frequencies of 4.7 and 120 ppm, respectively. For the direct dimension 1,024 complex data points were recorded, while 256 data points were recorded in the indirect dimension. The measuring times were 3.5 days for the 2D CAN, 1.5 days for the CON, 3 days for the 3D TROSY-HNCA, and 7 h for the $^{15}N^{1}$H-TROSY-HSQC

are a number of signals that are only observed in the CAN spectrum. These signals missing in the TROSY-HNCA are most likely from residues whose amides are not exchanged back to protons within a 4 days exposure to H_2O. Thus, the CAN experiment yields information that is not easily available from ^{1}H-detected triple resonance experiments due to incomplete amide back exchange in perdeuterated proteins expressed in D_2O. Thus, the experiment can be a valuable complement to conventional proton-detected triple resonance experiments. It is worth noting that only 83% of expected N–H correlations (189/227) are observed in ^{15}N-^{1}H TROSY-HSQC spectrum and of those 170

resonances were associated with a signal in the TROSY-HNCA spectrum, which was recorded with the same measuring time and concentration as the CAN spectrum (3.5 days, 1.5 mM). The total number of signals in the TROSY-HNCA spectrum was 272, which is comparable to the 250 in the CAN experiment. There are some correlations observed in the HNCA experiment that are not seen in the CAN for reasons not yet known. However, there are probably correlations missing in both experiments due to dynamic effects, which could only be answered by pursuing complete sequential assignments.

Finally, the nitrogen-detected experiments have superior resolution and signal overlap is much less severe than in the proton-detected experiments. A comparison with the TROSY-HSQC spectrum is shown in supplemental Fig. 4d. This is again due to the favorable relaxation properties of deuterated nitrogen nuclei, which is best exploited in the directly detected dimension.

Conclusion

In summary, the 2D CAN ^{15}N-direct-detection experiment provides an alternative way for establishing main chain resonance assignment of ^{15}N and $^{13}C^{\alpha}$ resonances using $^{13}C^{\alpha}$ chemical shift matching. On the other hand, the CON experiment takes advantage of the stronger CO–N coupling and can be used to complement assignments of backbone C′ atoms. Conventional uniform ^{13}C labeling is suitable for both the CAN and CON experiments. Unlike the NCA-DIPAP or NCO-IPAP experiments, which provide the same information using ^{13}C-direct detection, no complicated spin selection scheme is needed for the decoupling of the detected nuclei. In theory, the intensity (starting magnetization at the beginning of an FID) of the ^{15}N signal should be four-fold lower than that of a ^{13}C signal for an equal number of spins. In the CAN experiment, however, the sensitivity losses are largely compensated by the slower transverse relaxation of ^{15}N, a simpler and more efficient decoupling scheme, and the relaxation-optimized properties of the pulse sequences. For several types of residues such as Gly, Ser and residues with high-frequency C^{α}, significantly higher sensitivity was observed. Using slowly relaxing ^{15}N nuclei may be especially beneficial for assigning high molecular weight proteins. The experiments described here were recorded on a 500 MHz spectrometer and in D_2O to minimize the H–N dipole relaxation on ^{15}N nuclei. However, transverse relaxation of protonated ^{15}N in large proteins would be significantly reduced by cross-correlated relaxation caused by DD and CSA interference at higher magnetic fields (Pervushin et al. 1997). Thus, at higher magnetic fields and in H_2O solution, it may be very interesting to see the performance of this experiment slightly modified to exploit the TROSY effect. In addition, when compared to ^{1}H detected experiments, the CAN experiment as well as the CON experiments are not affected by the deuterium to proton exchange process which is often unsuccessful in large molecular weight proteins leading to incomplete assignments of the interior of the molecules. These experiments also have the ability of detecting Pro resonances. This feature is particularly important for the structural analysis of transcription activation factors as this class of proteins often contain proline-rich domain that are functionally important (Rao et al. 1997; Ruaro et al. 1997; Venot et al. 1998; Enkhmandakh et al. 2006). It is also known that large proteins that form biological switch functions often contain regulatory domains with phosphorylation sites, which are usually proline rich, partially folded and poorly understood. Examples are regulators of translation initiation, such as 4EBPs and their complexes with initiation factors (Marintchev et al. 2007). In addition, lower γ of the nuclei involved in the experiment are highly beneficial in approaching metal binding center of paramagnetic proteins. Thus, nitrogen detected experiments provide unique information not available in proton-detected experiments. Together with the superior resolution, the ^{15}N-detected CAN and CON experiments provide attractive alternatives and complements for assignment of backbone resonances.

Acknowledgments This work was supported by the NIH (grants AI37581, GM47467 and EB 002026).

References

Arnesano F, Banci L, Piccioli M (2005) NMR structures of paramagnetic metalloproteins. Q Rev Biophys 38:167–219

Balayssac S, Jimenez B, Piccioli M (2006) Assignment strategy for fast relaxing signals: complete aminoacid identification in thulium substituted calbindin D 9 K. J Biomol NMR 34:63–73

Bermel W, Bertini I, Felli IC, Kummerle R, Pierattelli R (2003) ^{13}C Direct detection experiments on the paramagnetic oxidized monomeric copper, zinc superoxide dismutase. J Am Chem Soc 125:16423–16429

Bermel W, Bertini I, Felli IC, Lee YM, Luchinat C, Pierattelli R (2006a) Protonless NMR experiments for sequence-specific assignment of backbone nuclei in unfolded proteins. J Am Chem Soc 128:3918–3919

Bermel W, Bertini I, Felli IC, Piccioli M, Pierattelli R (2006b) ^{13}C-detected protonless NMR spectroscopy of proteins in solution. Prog Nucl Magn Res Spec 48:25–45

Bermel W, Bertini I, Felli IC, Matzapetakis M, Pierattelli R, Theil EC, Turano P (2007) A method for Ca direct-detection in protonless NMR. J Magn Reson 188:301–310

Cai S, Seu C, Kovacs Z, Sherry AD, Chen Y (2006) Sensitivity enhancement of multidimensional NMR experiments by paramagnetic relaxation effects. J Am Chem Soc 128:13474–13478

Eletsky A, Moreira O, Kovacs H, Pervushin K (2003) A novel strategy for the assignment of side-chain resonances in

completely deuterated large proteins using 13C spectroscopy. J Biomol NMR 26:167–179

Emsley L, Bodenhausen G (1992) Optimization of shaped selective pulses for NMR using a quaternion description of their overall propagators. J Magn Reson 97:135–148

Enkhmandakh B, Makeyev AV, Bayarsaihan D (2006) The role of the proline-rich domain of Ssdp1 in the modular architecture of the vertebrate head organizer. Proc Natl Acad Sci USA 103:11631–11636

Ernst RR (1987) Principles of nuclear magnetic resonance in one and two dimensions. Oxford Science Publications, Oxford

Felli I, Brutscher B (2009) Recent advances in solution NMR: fast methods and heteronuclear direct detection. ChemPhysChem 10:1356–1368

Frueh DP, Arthanari H, Wagner G (2005) Unambiguous assignment of NMR protein backbone signals with a time-shared triple-resonance experiment. J Biomol NMR 33:187–196

Goddard TD, Kneller DG (2004) SPARKY 3 University of California, San Francisco

Grzesiek S, Bax A (1993) Amino acid type determination in the sequential assignment procedure of uniformly $^{13}C/^{15}N$-enriched proteins. J Biomol NMR 3:185–204

Hsu S-TD, Bertoncini CW, Dobson CM (2009) Use of protonless NMR spectroscopy to alleviate the loss of information resulting from exchange-broadening. J Am Chem Soc 131:7222–7223

Hyberts SG, Takeuchi K, Wagner G (2010) Poisson-gap sampling and forward maximum entropy reconstruction for enhancing the resolution and sensitivity of protein NMR Data. J Am Chem Soc 132:2145–2147

John M, Park AY, Dixon NE, Otting G (2006) NMR detection of protein ^{15}N spins near paramagnetic lanthanide ions. J Am Chem Soc 129:462–463

Kupče, Freeman R (1995) Adiabatic pulses for wideband inversion and broadband decoupling. J Magn Reson A 115:273–276

Kupče E, Freeman R, Wider G, Wüthrich K (1996) Figure of merit and cycling sidebands in adiabatic decoupling. J Magn Reson A 120:264–268

Lee D, Vögeli B, Pervushin K (2005) Detection of C′, Cα correlations in proteins using a new time- and sensitivity-optimal experiment. J Biomol NMR 31:273–278

Lin IJ, Xia B, King DS, Machonkin TE, Westler WM, Markley JL (2009) Hyperfine-shifted ^{13}C and ^{15}N NMR signals from costridium pasteurianum rubredoxin: extensive assignments and quantum chemical verification. J Am Chem Soc 131:15555–15563

Logan TM, Olejniczak ET, Xu RX, Fesik SW (1993) A general method for assigning NMR spectra of denatured proteins using 3D HC(CO)NH-TOCSY triple resonance experiments. J Biomol NMR 3:225–231

Machonkin TE, Westler WM, Markley JL (2004) Strategy for the study of paramagnetic proteins with slow electronic relaxation rates by NMR spectroscopy: application to oxidized human [2Fe-2S] ferredoxin. J Am Chem Soc 126:5413–5426

Marintchev A, Frueh D, Wagner G (2007) NMR methods for studying protein-protein interactions involved in translation initiation. Methods Enzymol 430:283–331

Marion D, Ikura M, Tschudin R, Bax A (1989) Rapid recording of 2D NMR spectra without phase cycling. Application to the study of hydrogen exchange in proteins. J Magn Reson 85:393–399

Pervushin K, Riek R, Wider G, Wüthrich K (1997) Attenuated T2 relaxation by mutual cancellation of dipole-dipole coupling and chemical shift anisotropy indicates an avenue to NMR structures of very large biological macromolecules in solution. Proc Natl Acad Sci USA 94:12366–12371

Rao A, Luo C, Hogan PG (1997) Transcription factors of the NFAT family: regulation and function. Annu Rev Immunol 15:707–747

Rovnyak D, Hoch JC, Stern AS, Wagner G (2004) Resolution and sensitivity of high field nuclear magnetic resonance spectroscopy. J Biomol NMR 30:1–10

Ruaro EM, Collavin L, Del Sal G, Haffner R, Oren M, Levine AJ, Schneider C (1997) A proline-rich motif in p53 is required for transactivation-independent growth arrest as induced by Gas1. Proc Natl Acad Sci USA 94:4675–4680

Serber Z, Richter C, Dötsch V (2001) Carbon-detected NMR experiments to investigate structure and dynamics of biological macromolecules. Chembiochem 2:247–251

Shaka AJ, Keeler J, Frenkiel T, Freeman R (1983) An improved sequence for broadband decoupling: WALTZ-16. J Magn Reson 52:335–338

Shaka AJ, Barker PB, Freeman R (1985) Computer-optimized decoupling scheme for wideband applications and low-level operation. J Magn Reson 64:547–552

Shimba N, Stern AS, Craik CS, Hoch JC, Dötsch V (2003) Elimination of ^{13}Calpha splitting in protein NMR spectra by deconvolution with maximum entropy reconstruction. J Am Chem Soc 125:2382–2383

Takeuchi K, Sun ZY, Wagner G (2008) Alternate ^{13}C–^{12}C labeling for complete main chain resonance assignments using Ca direct-detection with applicability toward fast relaxing protein systems. J Am Chem Soc 130:17210–17211

Takeuchi K, Frueh DP, Hyberts SG, Sun ZJ, Wagner G (2010) High-resolution 3D CANCA NMR experiments for complete main chain assignments using C_a direct-detection. J Am Chem Soc (in press)

Vance CK, Kang YM, Miller A-F (1997) Selective ^{15}N labeling and direct observation by NMR of the active-site glutamine of Fe-containing superoxide dismutase. J Biomol NMR 9:201–206

Vasos PR, Hall JB, Kummerle R, Fushman D (2006) Measurement of ^{15}N relaxation in deuterated amide groups in proteins using direct nitrogen detection. J Biomol NMR 36:27–36

Venot C, Maratrat M, Dureuil C, Conseiller E, Bracco L, Debussche L (1998) The requirement for the p53 proline-rich functional domain for mediation of apoptosis is correlated with specific PIG3 gene transactivation and with transcriptional repression. EMBO J 17:4668–4679